



## Original article

## Synthesis and evaluation of carbocyanine dyes as PRMT inhibitors and imaging agents

Sarmistha Halder Sinha<sup>a</sup>, Eric A. Owens<sup>a</sup>, You Feng<sup>a</sup>, Yutao Yang<sup>a</sup>, Yan Xie<sup>b</sup>, Yaping Tu<sup>b</sup>, Maged Henary<sup>a,\*</sup>, Yujun George Zheng<sup>a,\*\*</sup><sup>a</sup> Department of Chemistry, Georgia State University, PO Box 4098, Atlanta, GA 30302, USA<sup>b</sup> Department of Pharmacology, Creighton University, 2500 California Plaza, Omaha, NE 68178, USA

## ARTICLE INFO

## Article history:

Received 10 March 2012

Received in revised form

4 June 2012

Accepted 9 June 2012

Available online 21 June 2012

## Keywords:

Arginine methylation

PRMT

Inhibitor

Near-IR

Fluorescence

Carbocyanine

## ABSTRACT

Protein arginine methylation regulates multiple biological processes. Deregulation of protein arginine methyltransferase (PRMT) activities has been observed in many disease phenotypes. Small molecule probes that target PRMTs with strong affinity and selectivity can be used as valuable tools to dissect biological mechanisms of arginine methylation and establish the role of PRMT proteins in a disease process. In this work, we report synthesis and evaluation of a class of carbocyanine compounds containing indolium, benz[e]indolium or benz[c,d]indolium heterocyclic moieties that bind to the predominant arginine methyltransferase PRMT1 and inhibit its methyltransferase activity at low micromolar potencies. In particular, the developed molecules have long wavelength colorimetric and fluorometric photoactivities, which can be used for optical and near-infrared fluorescence imaging in cells or biological tissues. Together, these new chemical probes have potential application in PRMT studies both as enzyme inhibitors and as fluorescent dyes for microscope imaging.

© 2012 Elsevier Masson SAS. All rights reserved.

## 1. Introduction

Arginine methylation is a prevalent protein post-translational modification in cells, found in both nuclear and cytoplasmic proteins. This biochemical reaction is mediated by protein arginine methyltransferases (PRMTs) that utilize S-adenosyl-L-methionine (AdoMet, SAM) as the methyl donor to modify the guanidinium side chain of specific arginine residues, resulting in mono and dimethylated arginine residues and the coproduct S-adenosyl-L-homocysteine (AdoHcy, SAH). PRMTs are involved in the regulation of diverse biological processes ranging from structural remodeling of chromatin, gene transcription, RNA processing, DNA repair, translation, nucleocytoplasmic protein shuttling, nuclear hormone receptor-mediated signaling, to cell proliferation and differentiation [1–3]. Deregulation of PRMTs and arginine methylation has been reported to associate with a variety of human diseases including several types of tumors (e.g. breast cancer, prostate cancer, and leukemia) [4,5], pulmonary disorders [6] cardiovascular diseases [7,8] etc. In particular, the predominant

PRMT member, PRMT1, has been shown to impact a number of disease pathways. PRMT1 is an essential component of the mixed lineage leukemia (MLL) oncogenic transcriptional complex and confers an aberrant transcriptional activation property critical for the induction of leukemia [5]. Prominent roles of PRMT1 include the coactivation of nuclear receptors and regulation of hormone-dependent cancers [9,10]. Indeed, PRMT1 was found up-regulated in breast cancer concomitantly with a change in substrate methylation [11]. PRMT1 variant 1 expression may be used as a marker of unfavorable prognosis for breast cancer patients [12]. PRMT1 variant 2 was regarded as a marker of unfavorable prognosis in colon cancer patients [13]. Thus, targeting PRMT activities with small molecule inhibitors could be an effective therapeutic strategy in new drug development [3,14,16]. Indeed, quite a few research efforts have been investigated in the past years in attempt to develop potent and selective PRMT inhibitors [15–28].

Carbocyanine dyes are unique organic molecules that contain a conjugated electron-deficient system between two heterocyclic nitrogen atoms that provides characteristically long absorption and emission wavelengths; the associated wavelengths of carbocyanine dyes have been exploited in many applications [29,30]. Using various synthetic methods, the conjugated system of these compounds can be altered to assume specific absorption and fluorescence spectra in the range of 400–1000 nm [31,32]. The

\* Corresponding author. Tel.: +1 404 413 5566; fax: +1 404 413 5505.

\*\* Corresponding author. Tel.: +1 404 413 5491; fax: +1 404 413 5505.

E-mail addresses: [mhenary1@gsu.edu](mailto:mhenary1@gsu.edu) (M. Henary), [yzheng@gsu.edu](mailto:yzheng@gsu.edu) (Y.G. Zheng).

number of carbon atoms between the heterocyclic nitrogen atoms in the polymethine chain determines the common name for the dyes. In particular, penta- and heptacarbocyanine dyes (5 and 7 carbon atoms, respectively) have been extensively utilized for binding analyses; however, trimethine cyanine dyes (3 carbon atoms) remain, until recently, unexplored [33]. Trimethine cyanine dyes commonly absorb and emit light in the visible region; however, varying the conjugated heterocyclic moieties greatly shifts the maximum absorption and emission wavelengths. Their binding properties to biomolecules can be studied using relative spectrophotometric changes either in absorption or emission spectra [34]. In this study, we synthesized and identified a set of trimethine cyanine dyes that specifically inhibit the enzymatic activity of PRMT1. Also, a proof-of-principle study has demonstrated that these molecules are well suited for colorimetric and fluorescent imaging of PRMT activities in living cells. Overall, the identified carbocyanine molecules with unique photoactive properties could be powerful chemical probes in elucidating mechanisms and functions of PRMTs underlying different biological or pathological contexts.

## 2. Results and discussion

### 2.1. Chemistry

Toward the development of PRMT inhibitors and imaging agents, we have concentrated on hydrophobic trimethine cyanine derivatives utilizing ethyl, butyl and phenylpropyl halides for nitrogen alkylation of the heterocyclic indolium, benz[e]indolium and benz[c,d]indolium moieties (Schemes 1 and 2). The synthetic sequence to NIR trimethine cyanine dyes **11–13** involves 6 steps as shown in Scheme 1. The key step is the formation of 5-(benz[c,d]

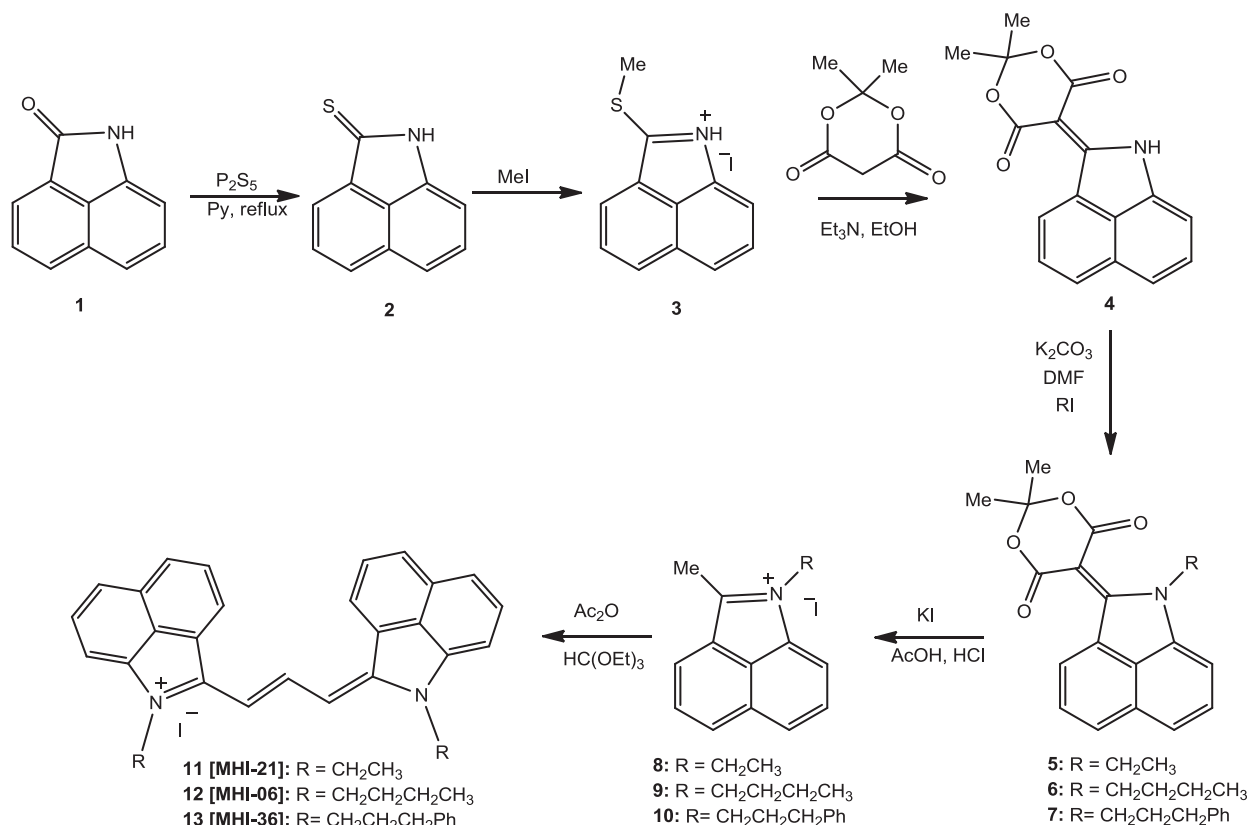
indol-1*H*-2-ylidene)-1,3-dioxane-4,6-dione **4**. The alkylation of **4** provides an easy access to various 1-alkyl-substituted 2-methylbenz[c,d]indolium salts, the important precursors to a set of various carbocyanine dyes.

Benz[c,d]indole derivatives **2–4** were synthesized starting with the commercial substrate **1**. Compound **4** was reacted with various alkyl iodides under basic conditions to afford esters **5–7**, which were correspondingly transformed into various quaternary salts **8–10**. Salts **8–10** were purified by crystallization from methanol. The condensation of **8–10** with triethyl orthoformate in Ac<sub>2</sub>O furnished the benz[c,d]indolium trimethine cyanine dyes **11–13** in very good yield.

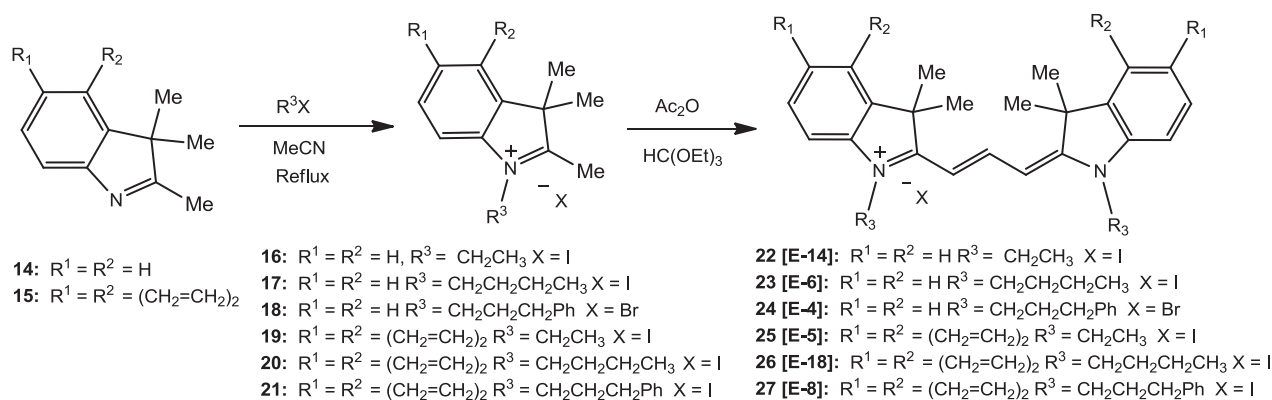
Additionally, trimethine cyanines containing slightly varied heterocyclic end units, indolium **14** and benz[e]indolium **15**, were synthesized as depicted in Scheme 2. Using similar chemistry, as outlined in Scheme 1, quaternization of commercially obtained indolium and benz[e]indolium **14–15** proceeds by a S<sub>N</sub>2 reaction using corresponding alkyl halides in boiling acetonitrile to yield salts **16–21** corresponding to starting heterocyclic subunits. Trimethine cyanines **22–27** were synthesized in good yield under identical reaction conditions depicted in Scheme 2. Final trimethine cyanines were purified by recrystallization from methanol or column chromatography using 2% MeOH in DCM as eluting solvent. Experimental procedures for novel compound preparation, chemical and physical spectroscopic data are reported in the Supplemental information.

### 2.2. Biochemical identification of the carbocyanine inhibitors of PRMT1

In an effort to discover potent and selective PRMT inhibitors, we synthesized and investigated several trimethine cyanine compounds



Scheme 1.



Scheme 2.

by screening their anti-methyltransferase activity. Our initial hypothesis developed from the rationale that carbocyanine molecules typically display heteroatomic and cationic structures, which could potentially resemble positively charged arginine residues in protein substrates, thereby leading to competitive PRMT inhibitors. One of the characteristic features of carbocyanine molecules is their absorption and fluorescence emission in the near-IR range which offers a great advantage for *in vivo* fluorescent imaging with minimal background interference from biomolecular autofluorescence. In the inhibitor screening study, we selected PRMT1 as the primary target because it is the predominant PRMT isoform found in mammalian cells and is involved in many key biological processes. In a typical anti-arginine methyltransferase screening assay, the reaction mixture involved carbocyanine compounds, recombinantly expressed His-tagged PRMT1, [ $^{14}C$ ]-labeled AdoMet, and a histone H4 peptide containing the 20-amino acid sequence on the N-terminal tail of histone H4, i.e. H4-20. The reaction was conducted at 30 °C in a volume of 30  $\mu$ L. The degree of diminishment in PRMT1 activity was used as a parameter to evaluate the potency of the compounds in inhibiting PRMT1-mediated arginine methylation. In a more quantitative analysis of the inhibition potency, we measured the methyltransferase activity of the enzyme at a range of concentrations of inhibitors and  $IC_{50}$  values were derived from the dose response curve as the half-inhibition concentration. For all the enzymatic assays, the methylation reaction was controlled under the initial condition so that the reaction yields of the limiting substrates were lower than 15%, which was to ensure that the concentrations of AdoMet and peptide substrate did not decrease significantly over the time course of methylation reaction. This procedure also prevented potential product inhibition from SAH.

From the biochemical screening, we found three structurally related trimethine cyanine compounds that show desired anti-PRMT1 activity; the chemical structures and corresponding  $IC_{50}$  values are shown in Table 1 (Group A). Clearly these compounds are structurally analogous, all of which contain a delocalized positive charge on the nitrogen atom and two benz[c,d]indolium moieties at the ends of the trimethine cyanine main chain. The inhibition potency is in the order of **11** > **12** > **13**. This could possibly suggest that increasing the size of the N-substituent causes increasing steric hindrance, which prevents the compound from entering the inhibitor-binding site of the enzyme. Interestingly, **11** (MHI-21) shows the smallest size but best inhibition potency with  $IC_{50}$  of 4.1  $\mu$ M, which warrants further investigation.

To further this study, we synthesized and tested another set of carbocyanine compounds containing an indolium group as the heterocyclic moiety in order to screen for more potent inhibitors and explore possible structure–activity relationship (SAR) (Group B in Table 1). Compared to the above three benz[c,d]indolium

containing dyes, this set of compounds with the exception of **24** presented significantly weaker activity.  $IC_{50}$  values of **22**, **23**, **28** and **29** were all greater than 150  $\mu$ M. For **30** and **31**, at 100  $\mu$ M concentration, PRMT1 still retained 80–95% of its activity. These data demonstrate that reducing the heterocyclic size generally lowers the binding of the carbocyanine molecules to PRMT1. Notably, the two molecules that harness additional positive charges on the N-substitution group, i.e. **28** and **29**, do not offer any advantage for enhancing the inhibition potency. This indicates that charge alone is not the sole factor that determines the specific inhibitor–enzyme interactions, as a certain degree of hydrophobicity of the N-substitution is required for efficient inhibition. Contrary to the benz[c,d]indolium trimethine compounds (Group A in Table 1), longer and bulky substituents on the heterocyclic ring nitrogen increase inhibition potency. In particular, **24** having a bulky phenylpropyl substituent showed the strongest potency, with  $IC_{50}$  of 6.3  $\mu$ M. This may suggest that a bulky hydrophobic group either on the heterocyclic ring moiety or on the heterocyclic ring nitrogen substitution is required for effective binding to PRMT1 protein.

To provide more information on the effect of the heterocyclic moiety, we synthesized and tested three other trimethine cyanine analogs bearing the benz[e]indolium end unit (Group C in Table 1) while maintaining the identical set of nitrogen substituents, i.e., ethyl, butyl, and phenylpropyl group. The potency of benz[e]indolium cyanines becomes weaker than the benz[c,d]indolium cyanines that contain the same substituent. For instance, comparing the ethyl-substituted compounds bearing the benz[e]indole **25** ( $IC_{50}$  of 20.3  $\mu$ M) and the benz[c,d]indole **11** ( $IC_{50}$  of 4.1  $\mu$ M) indicates that the position of the benz group attached on the heterocyclic ring affects inhibitor–enzyme interaction. Also, the weaker binding of benz[e]indolium is rescued by the incorporation of a bulky phenylpropyl substituent on the heterocyclic nitrogen; this is observed as the inhibition potency increases from **25** to **27**. In contrast, in benz[c,d]indolium-containing cyanine compounds, the end head group seems to dominate the inhibitor–PRMT1 binding and the bulky substitutions on the heterocyclic nitrogen do not offer any positive contributions (i.e. **36**).

### 2.3. Noncompetitive inhibition by **11**

The finding that certain trimethine cyanine compounds exhibit low micromolar anti-PRMT1 activity is encouraging. Especially, **11** shows the smallest molecule size but the strongest potency in the tested compounds; the other one having similar potency to **11** is **24** (E-4). Thus, we next carried out more detailed analyses of PRMT1 inhibition by **11** in order to understand the inhibitory mechanism of this type of carbocyanine molecules.

**Table 1**The names, structures and IC<sub>50</sub> data of trimethine cyanine compounds.

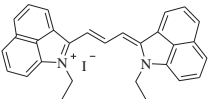
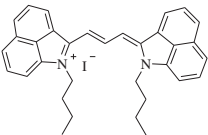
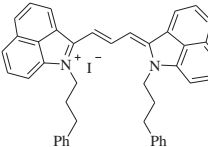
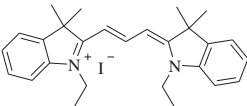
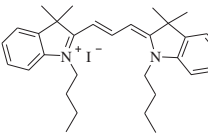
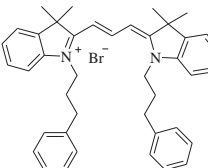
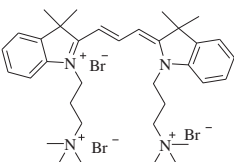
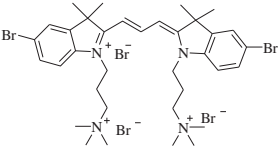
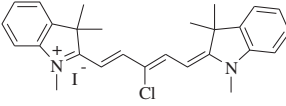
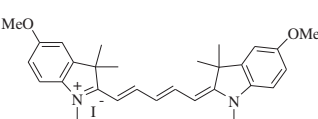
Type of compound	Name	Structure	IC <sub>50</sub> ( $\mu$ M)
Group A  Trimethine cyanine compounds containing benzo[c,d]indolium groups in the two ends	<b>11</b> [MHI-21]		4.1 $\pm$ 0.1
	<b>12</b> [MHI-06]		12.0 $\pm$ 0.5
	<b>13</b> [MHI-36]		15.5 $\pm$ 0.2
Group B  Trimethine cyanine compounds containing indolium groups in the two ends.	<b>22</b> [E-14]		284.2 $\pm$ 3.5
	<b>23</b> [E-6]		160.8 $\pm$ 1.2
	<b>24</b> [E-4]		6.3 $\pm$ 0.3
	<b>28</b> [A-C3]		368.3 $\pm$ 25.9
	<b>29</b> [A-N3]		291.7 $\pm$ 40.1
	<b>30</b> [MHI-106]		At 100 $\mu$ M concentration 80% activity retained
	<b>31</b> [MHI-128]		At 100 $\mu$ M concentration 95% activity retained

Table 1 (continued)

Type of compound	Name	Structure	IC <sub>50</sub> ( $\mu$ M)
Group C Trimethine cyanine compounds containing benzo[e]indolium group as the end units	25[E-5]		20.3 $\pm$ 0.2
	26[E-18]		18.0 $\pm$ 0.5
	27[E-8]		14.3 $\pm$ 0.2

First, we conducted steady-state enzymatic measurements to analyze the kinetic pattern of inhibition by **11**. The initial velocities of PRMT1 were measured at several selected concentrations of the inhibitor over a range of varied concentrations of one substrate while fixing the concentration of the other. The kinetic inhibition data points were analyzed by fitting to the linear competitive or noncompetitive inhibition equations. The data were plotted in the double reciprocal format with  $1/\text{velocity}$  versus  $1/\text{concentration}$  of the varied substrate (Fig. 1). It is seen that in both double–reciprocal plots, a series of straight lines intersect at a point in the second quadrant. These data demonstrate that **11** is a noncompetitive inhibitor with regard to both H4 and AdoMet substrates.

#### 2.4. Reversible vs irreversible inhibition

To determine whether **11** reversibly or irreversibly inhibits PRMT1 enzyme, a dialysis experiment was performed. For each assay, fixed amounts of enzyme and inhibitor were incubated at 30 °C for 1 h to allow for enzyme inactivation. Then the solution

was dialyzed against the assay buffer for 72 h. The methyltransferase activity of PRMT1 before and after dialysis was measured using the filter binding method. As shown in Fig. 2A, in the presence of 20  $\mu$ M **11**, PRMT1 only retained 10% activity prior to dialysis. After dialysis, the enzyme activity was restored to 66% suggesting that PRMT1 inhibition by **11** is reversible. To confirm this result, we measured time-dependent inhibition at several concentrations of the inhibitor (0, 1.5, 2.5, 4.0  $\mu$ M). In the time vs product plot (Fig. 2B), straight lines were seen for all the measurements instead of hyperbolic curves. Lack of any nonlinear time-dependent inhibition indicates that the inhibition is reversible and there is no covalent interaction between PRMT1 and the inhibitor.

#### 2.5. Binding model analysis of inhibitor–enzyme interaction

To understand the structural basis of PRMT1 inhibition by **11**, we performed a docking study of the compound with PRMT1 structure using the program Autodock. A homology model of human PRMT1

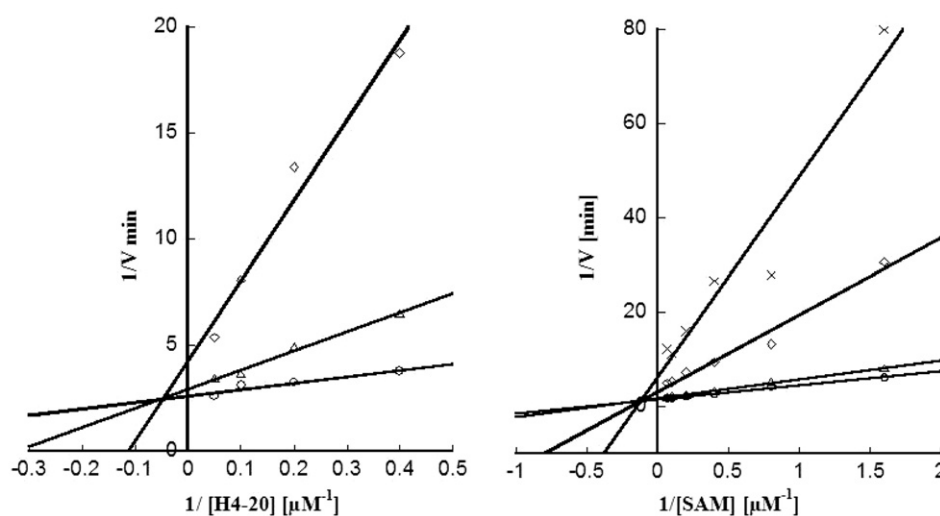


**Fig. 1.** Steady-state kinetic analysis of PRMT1 inhibition by **11**. (A) Double–reciprocal plot of the initial velocities versus H4 peptide with AdoMet concentration fixed at 5  $\mu$ M and with varied concentrations of **11** at 2.5  $\mu$ M (O), 5  $\mu$ M ( $\Delta$ ), and 7.5  $\mu$ M ( $\diamond$ ). (B) Double–reciprocal plot of the initial velocities versus AdoMet with H4-20 concentration fixed at 2  $\mu$ M and with varied concentrations of **11** at 0  $\mu$ M (O), 2.5  $\mu$ M ( $\Delta$ ), 5  $\mu$ M ( $\diamond$ ), and 6.5  $\mu$ M ( $\times$ ).



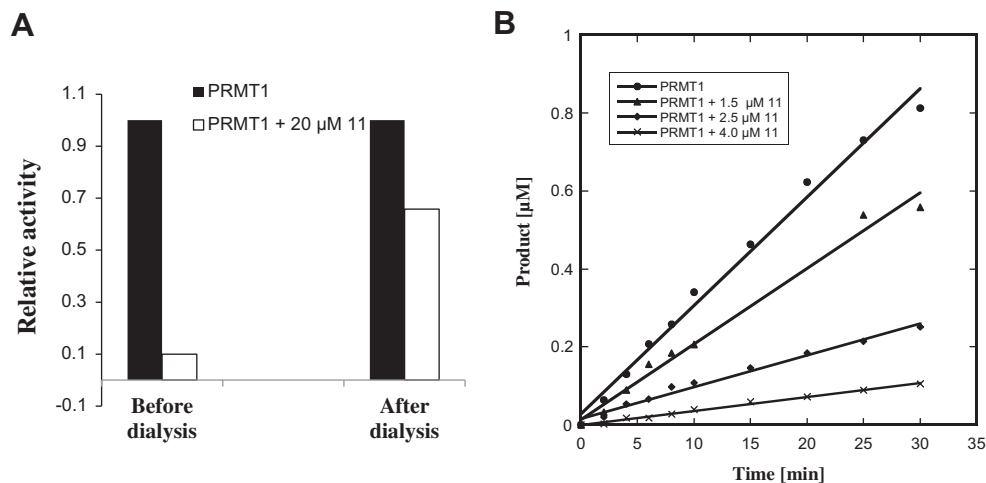


**Fig. 2.** Test of the reversibility of PRMT1 inhibition by **11**. (a) Dialysis experiment in presence and absence of **11**. (b) Progression assay of PRMT1 inhibition at different concentrations (1.5, 2.5, and 4.0  $\mu$ M) of **11**.

structure was created from rat PRMT3. In the docking, a grid box was created to cover the whole protein structure. The docking result was analyzed according to the lowest energy order. As it turned out, the docked ligand was found to distribute predominantly in three regions on the protein surface (Fig. 3A); none of them overlap with the arginine and SAM binding sites. Therefore **11** is likely an allosteric inhibitor. These results are in agreement with the kinetic results, which showed noncompetitive inhibition in respect to H4-20 and AdoMet. For a more accurate analysis of the binding mode, the compound was individually docked in each of the three regions by choosing a grid box covering only that selected region. A close inspection on region 1 revealed that **11** binds to

a pocket formed by Glu 19, Tyr 35, Ser 38, Tyr 39, Glu 47, Met 48, Tyr 148, Tyr 152, Val 206, Pro 217, His 293, Lys 295, Thr 297, Arg 327, Met 352 and Arg 353 residues (Fig. 3B). The inhibitor electrostatically interacts with residues Glu 19 and Glu 47, and makes hydrogen bond contacts with Ser 38, Tyr 39, Tyr 148, Tyr 152, Lys 295, Thr 297, Met 352 and Arg 353. The hydroxyl group of Tyr 148 seems to have a strong H-bonding interaction with two nitrogens of **11** (3.7 Å and 4.3 Å) and a moderate interaction with Tyr 152 (6.7 Å and 7.0 Å). A detailed study on region 2 shows that the compound binds to the pocket formed by residues Leu 49, His 45, Gly 80, Thr 81, Gly 82, Ile 83, Met 86, Phe 87, Asn 102, Tyr 107, and Ile111 and makes hydrogen bond interactions with Phe 42, His 45, Gly 80, Thr 81, Gly 82, Ile 83,

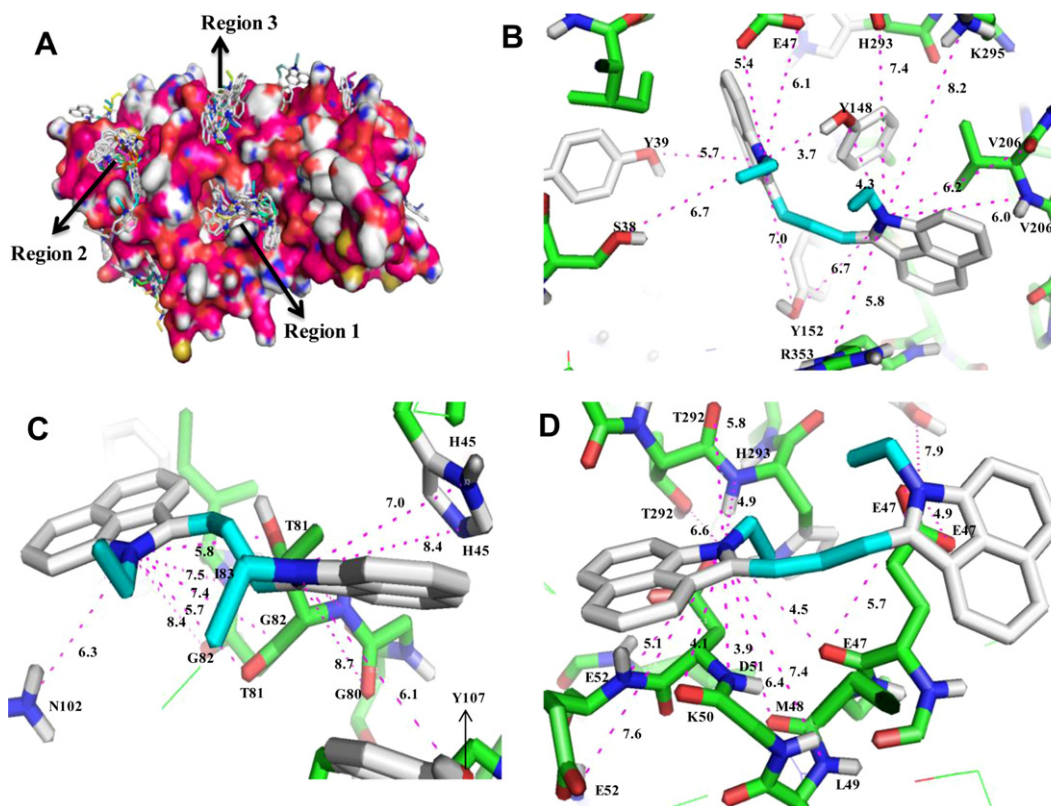


**Fig. 3.** Docking results. (A) Probable binding regions of **11**. Binding mode of the inhibitor in Region 1 (B), in Region 2 (C), and in Region 3 (D).

Met 86 and Tyr 107 residue (Fig. 3C). There is a moderate H-bonding interaction between the heterocyclic nitrogen of the compound and the side chain and backbone oxygen atoms of Thr 81, with 5.8 Å, 5.7 Å, respectively. Similar docking study on region 3 revealed that the compound binds to the pocket formed by Glu 47, Met 48, Leu 49, Lys 50, Glu 52, Val 53, Tyr 148, Pro 290, Tyr 291, Thr 292 and His 293 residue and makes several electrostatic interactions with residues Glu 47, Asp 51, Glu 52, and hydrogen bond interaction with Lys 50, Met 48, Leu 49, Glu 52, Val 53, Pro 290, Tyr 291, and Thr 292 (Fig. 3D). Together, the inhibitory activity of **11** may come from its single or combined interactions at the three major binding sites of PRMT1.

## 2.6. Investigation of interaction of **11** and PRMT1 using site-directed mutagenesis

To test the validity of the docking results, site-directed mutagenesis was conducted to mutate the residues predicted to interact with the compound in the docking model. Since multiple hydrogen bonding interactions occur between the side chains of Tyr 148, Tyr 152, Thr 81 and Thr 292 residues and the heterocyclic ring nitrogen atom of **11**, we introduced four mutations, i.e., Y148A, Y152A, T81A, T292A. All these PRMT1 mutants were produced using QuikChange site-directed mutagenesis protocol, expressed in *Escherichia coli*, and purified by Ni-NTA affinity chromatography. Activity of each mutant protein was examined by the radioactive methyltransferase assay in which recombinant PRMT1, [<sup>14</sup>C] AdoMet, and H4-20 were incubated at 30 °C in the presence or absence of 4 μM **11**. The retained fractional activity was quantified to evaluate the inhibition potency of the inhibitor on each PRMT mutant (Fig. 4). It is seen that the activities of Y148A, T81A and T292A protein were inhibited by **11** by ≈ 60%, 65% and 70% respectively, less than that of wild type PRMT1 (92%). These results support that Y148, T81 and T292 residues might interact with **11** and thus mutation of these residues decreased the binding and inhibition. **11** inhibited Y152A mutant with same potency as is for wt-PRMT1, which signifies that Y152 quite likely is not involved in interaction with **11**.

## 2.7. Selectivity of **11**

We then investigated whether **11** is selective for PRMT1 inhibition. For this study, we examined the inhibition by **11** of several other PRMT isoforms, PRMT3, PRMT4/CARM1, PRMT5, and PRMT6, using the radioactive methyltransferase assays. The IC<sub>50</sub> values are shown in Table 2. PRMT3 was inhibited at IC<sub>50</sub> of 8.3 ± 0.1 μM,

**Table 2**

Comparison of the inhibition of PRMT1, -3, -4, -5 and -6 by **11**.<sup>a</sup>

	Peptide substrate	IC <sub>50</sub> (μM)
His6x-rPRMT1	H4(1–20)	4.1 ± 0.1
His6x-PRMT3	R4	8.3 ± 0.1
GST-CARM1	H3(1–31)	≈ 100
His6x-PRMT5	H4(1–20)	9.1 ± 1.0
His6x-PRMT6	H3(1–31)	12.6 ± 1.1

<sup>a</sup> Data obtained from the results of the radioactive methylation assays with varied concentrations of **11**. For inhibition of His6x-PRMT1, 2 μM H4(1–20), 5 μM [<sup>14</sup>C]-SAM, and 0.05 μM enzyme were used. For inhibition of His6x-PRMT3, 2 μM R4, 5 μM [<sup>14</sup>C]-SAM, and 0.1 μM enzyme were used. For inhibition of GST-CARM1, 1 mM H3(1–31), 30 μM [<sup>14</sup>C]-SAM, and 5 μM enzyme were used. For inhibition of His6x-PRMT6, 10 μM H3(1–31), 5 μM [<sup>14</sup>C]-SAM, and 0.5 μM enzyme were used.

about 2.0 fold higher than PRMT1. **11** inhibits PRMT5 at IC<sub>50</sub> 9.1 ± 1.0 μM which is about 2.2 fold higher than PRMT1. The IC<sub>50</sub> of **11** for CARM1 is particularly higher, ~100 μM. **11** inhibits PRMT6 with an IC<sub>50</sub> of 12.6 μM, 3.1-fold higher than PRMT1. Overall, **11** seems to inhibit all the tested PRMT proteins, with a little preference observed for PRMT1. The variation in inhibition potency likely is caused by the subtle differences between the structures of individual PRMT members.

## 2.8. Evaluation of the cellular activity of **11**

After the biochemical characterizations, we moved on to examine possible cellular effects of **11**. We first examined subcellular distribution of **11** in HeLa cells. A marked feature of carbocyanine compounds is their spectral absorption and fluorescence emission in the near-IR region. Measured in methanol, **11** has absorption maximum at 758 nm and emission maximum at 774 nm. Interestingly, after incubation with **11** for 6 h, cells showed bright, blue-colored staining and can be viewed directly under bright field microscope. Microscopic images shown in Fig. 5A–C demonstrated that **11** was concentrated in the nucleus of HeLa cells in a dose dependent manner and a small amount of **11** was also found in the cytoplasmic vesicles. Since carbocyanine compounds have fluorescent emission in the long wavelength region, we performed near-infrared fluorescent imaging of HeLa cells by confocal microscopy using a 633 nm laser for fluorescence excitation and a 715–785 nm Long Pass for emission. As can be seen in Fig. 5E and F, after 6-h incubation in HeLa cells, the compound was concentrated around nucleus or in the nucleus and a low level was in the cytoplasmic vesicles. The result is consistent with the light microscopic images. As expected, the control HeLa cells treated with DMSO did not show any fluorescent signal (Fig. 5D).

We next studied the growth inhibitory effect of **11** in HeLa cells by using the MTT assay. The HeLa cells were cultured for 40 h in the presence of different doses of **11** (Fig. 6). From the data, EC<sub>50</sub>, the concentration of the compound required to reduce the cell survival level to 50% at 48 h of exposure, was determined to be 0.94 ± 0.09 μM. This value is remarkably lower than the IC<sub>50</sub> value (i.e. 4.1 μM) measured in the biochemical assay, likely suggesting that **11** easily penetrates the plasma membrane and subsequently affects the cell proliferation. To better understand the mechanism underlying the observed proliferation inhibition, we examined the effect of **11** on cell cycle of HeLa cells. The subpopulations of propidium iodide-stained HeLa cell were determined using flow cytometry at varying concentrations of the compound in a time dependent manner. Untreated HeLa cells showed a pattern of cell growth phase distribution at G1 (57.2%), S (12.2%) and G2/M (29.2%). With increasing doses (e.g. 0.3, 1, 2.5 and 5 μM) at 24 h, S phase arrest was shown to occur with a concomitant decrease of

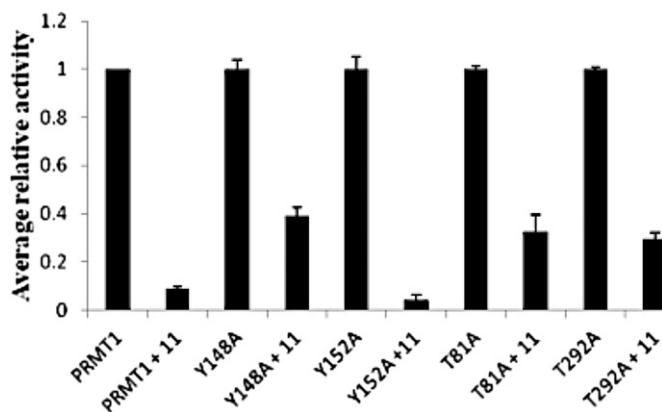


**Fig. 4.** Inhibition of the activity of WT- and mutant- PRMT1 by **11**. The reaction contained 2 μM H4-20, 5 μM [<sup>14</sup>C] AdoMet and 4 μM inhibitor. Activities of all PRMT1 mutants were normalized to the same level as that of wt-PRMT1 for clear comparison.

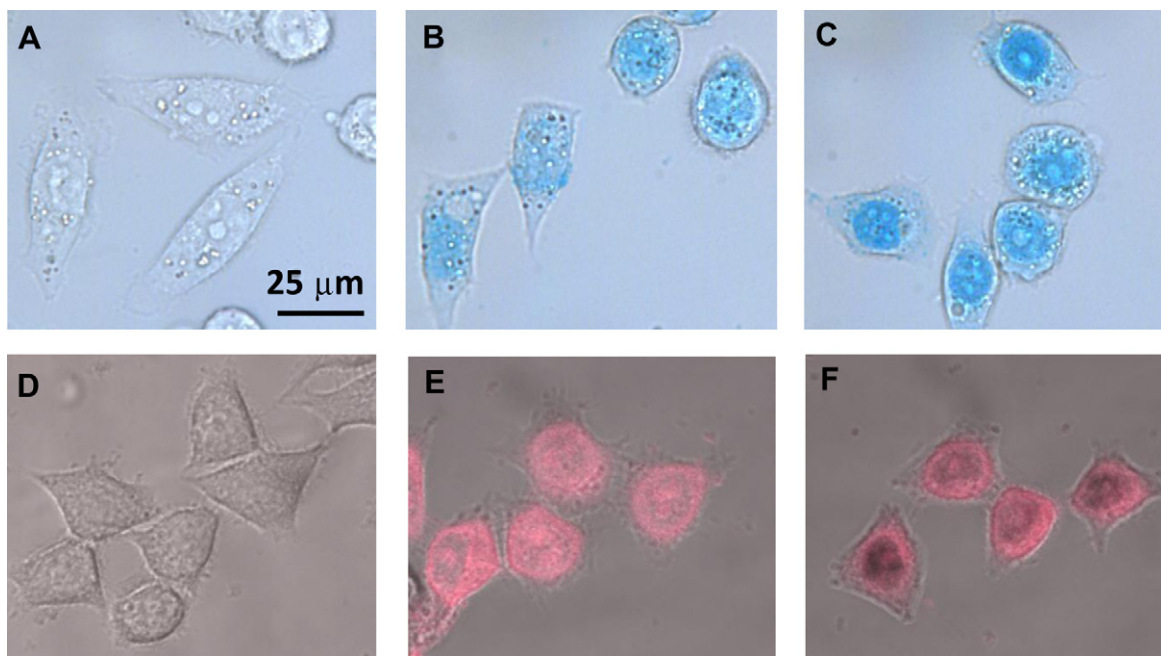


**Fig. 5.** Microscopic imaging of **11** in HeLa Cells. HeLa cells are treated with 0 (control), 2, and 5  $\mu\text{M}$  of **11**. Figures A, B and C are the optical images of HeLa cells captured under visible light by CoolSNAP CF camera attached to a Nikon Ti-80 microscope. Figures D, E and F are fluorescent images of HeLa cells captured by fluorescence confocal microscopy. (For interpretation of the references to colour in this figure legend, the reader is referred to the web version of this article.)

cell populations in the other phases of the cell cycle (Fig. 7) In particular, S phase cell population increased from 12.2% to 56.5% at 1  $\mu\text{M}$  **11**. Under this condition, the G1 cells decreased from 57.2% in the control to 23.6% and the G2/M phase cells decreased from 29.2% to 13.9%. The increase in S phase likely suggests that **11** enters the nucleus and causes chromatin dysfunction, so that the spindles fail to assemble which requires DNA damage to be repaired before proceeding to the G2/M phase. After 48 h of treatment at 2.5 and 5  $\mu\text{M}$  **11**, appearance of a hypodiploid peak (Sub-G1) was observed, indicative of apoptosis (data not shown).

### 3. Conclusions

PRMT proteins play functional roles in a wide variety of diseased phenotypes, and therefore the development of novel potent small molecule inhibitors of PRMTs is highly desired for both basic and applied pharmacology. We synthesized carbocyanine molecules

containing different heterocyclic moieties and hydrophobic substituents, and identified several possessing micromolar potency for PRMT1 inhibition. In particular, compound **11** presents potent inhibitory activity on PRMT1, with  $\text{IC}_{50}$  of 4.1  $\mu\text{M}$ . We have demonstrated that this compound is a noncompetitive inhibitor, and combined with docking simulation and site mutagenesis analysis, we suggest **11** likely targets an allosteric site(s) in PRMT1. Selectivity study showed that the compound has certain specificity toward PRMT1 inhibition. The cyanine molecules typically possess long-wavelength absorption and fluorescence properties which allow them to be used for visualization in cells and tissues. By using the optical and fluorescent microscopies, cell proliferation, and flow cytometry assays, we found that **11** is capable of crossing the plasma membrane, staying in the nucleus and interfering with the chromatin function. Together, this study provides unique photoactive chemical probes for both PRMT inhibition and microscopic imaging.

### 4. Experimental methods

#### 4.1. Chemicals

Most chemical reagents were obtained from Sigma Aldrich. Melting points (open Pyrex capillary) were measured on a Mel-Temp apparatus and are uncorrected.  $^1\text{H}$  NMR and  $^{13}\text{C}$  NMR spectra were recorded on either Bruker Avance (400 MHz) or a Varian Unity+300 (300 MHz) spectrometer using  $\text{DMSO}-d_6$  or  $\text{MeOD}-d_4$  containing tetramethylsilane (TMS) as an internal standard. Vis/NIR absorption spectrum was recorded on a Varian Cary 50 spectrophotometer. High-resolution accurate mass spectra (HRMS) were obtained using a Waters Q-TOF micro (ESI-Q-TOF) mass spectrometer.

#### 4.2. Benz[c,d]indole-2(1H)-thione (**2**)

This compound was obtained in a 93% yield; mp 146–148  $^{\circ}\text{C}$ ; (reported: yield 82%, mp 156  $^{\circ}\text{C}$ .) [35–37].

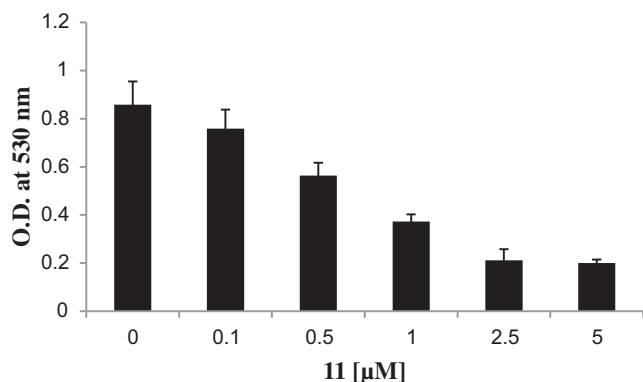


**Fig. 6.** The antiproliferation effect of **11** in HeLa Cells. Cells were treated with different concentrations of **11** as indicated for 48 h and O.D. at 530 nm was measured using MTT assay. Data are presented as the average of three independent experiments.



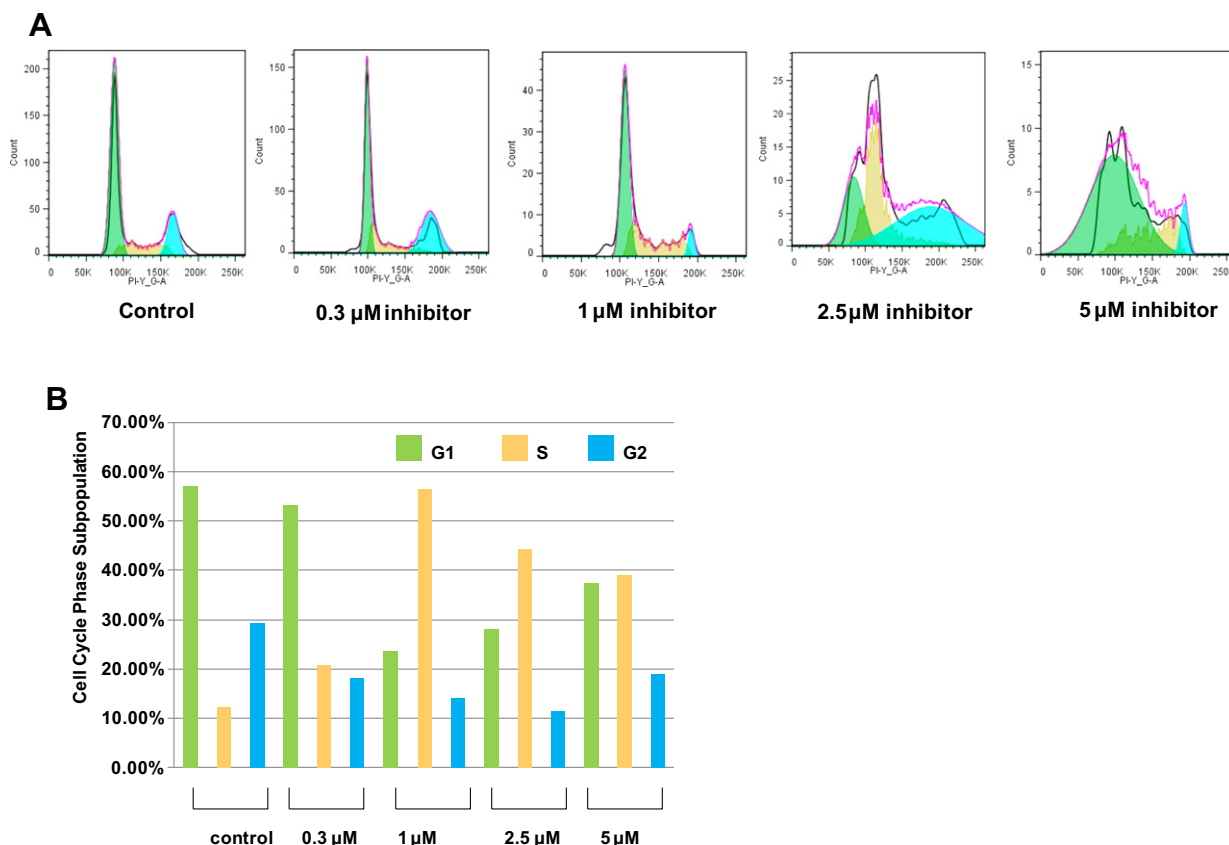


**Fig. 7.** Cell cycle analysis of HeLa cells treated with different doses of **11**. Data are presented as the relative fluorescence intensity of cell subpopulations in the FACS profile (panel A) and as percentage of cell subpopulations under each condition (panel B).

#### 4.3. 2-Methylthiobenz[*c,d*]indole hydroiodide (**3**)

This compound was prepared using the reported procedures [36,38]. Since the product was unstable, it is used in the next step without further purification.

#### 4.4. 2-(2,2-Dimethyl-4,6-dioxo-1,3-dioxane-5-yliden)-1H-benz[*c,d*]indole (**4**)

This compound was obtained in an 85% yield; mp 220 °C; (reported: yield 94%, mp 223 °C) [36,37].

#### 4.5. General procedures of the synthesis of compounds **5–7**

A mixture of compound **4** (10.2 mmol), alkyl iodide (30.6 mmol) and K<sub>2</sub>CO<sub>3</sub> (30.6 mmol) were heated in DMF (40 mL) at 90 °C for 18 h under a nitrogen atmosphere. The mixture was cooled to room temperature and then filtered. The filtrate was concentrated under reduced pressure. The residue was purified on silica gel (flash column chromatography, using EtOAc–hexanes, 1:2 as an eluent).

##### 4.5.1. 1-Ethyl-2-(2,2-dimethyl-4,6-dioxo-1,3-dioxan-5-ylidene)-1H-benz[*c,d*]indole (**5**)

Yield 65%, mp 183–184 °C; <sup>1</sup>H NMR (300 MHz, DMSO-*d*<sub>6</sub>) δ 1.46 (t, *J* = 7.0 Hz, 3H), 1.70 (s, 6H), 4.39 (q, *J* = 7.0 Hz, 2H), 7.78 (m, 1H), 7.91 (m, 2H), 8.01 (m, 1H), 8.40 (d, *J* = 8.0 Hz, 1H), 8.90 (d, *J* = 8.0 Hz, 1H).

##### 4.5.2. 1-Butyl-2-(2,2-dimethyl-4,6-dioxo-1,3-dioxan-5-ylidene)-1H-benz[*c,d*]indole (**6**)

Yield 74%, <sup>1</sup>H NMR (300 MHz, DMSO-*d*<sub>6</sub>) δ 0.86 (t, *J* = 7.5 Hz, 3H), 1.27 (q, *J* = 7.2, 2H), 1.75 (s, 6H), 1.82 (p, *J* = 6.6 Hz, 2H), 3.39 (t,

*J* = 7.5 Hz, 2H), 7.79 (t, *J* = 7.5 Hz, 1H), 7.94 (t, *J* = 7.8 Hz, 1H), 8.02 (d, *J* = 7.2 Hz, 1H), 8.06 (d, *J* = 8.4 Hz, 1H), 8.45 (d, *J* = 8.1 Hz, 1H), 8.91 (d, *J* = 7.2 Hz, 1H).

##### 4.5.3. 1-Phenylpropyl-2-(2,2-dimethyl-4,6-dioxo-1,3-dioxan-5-ylidene)-1H-benz[*c,d*]indole (**7**)

Yield 92%, mp 155–157 °C; <sup>1</sup>H NMR (400 MHz, DMSO-*d*<sub>6</sub>) δ 2.17 (m, 2H), 2.56 (t, *J* = 7.0 Hz, 2H), 4.35 (t, *J* = 7.0 Hz, 2H), 7.17 (m, 5H), 7.71 (d, *J* = 7.5 Hz, 1H), 7.86 (m, 2H), 7.88 (t, *J* = 7.5 Hz, 1H), 8.38 (d, *J* = 8.0 Hz, 1H), 8.88 (d, *J* = 8.0 Hz, 1H).

#### 4.6. General procedures of the synthesis of salts **8–10**

Ester **5–7** (2.9 mmol) was dissolved in acetic acid (4 mL) and the mixture was refluxed for 20 min. Concentrated HCl (4 mL) was added dropwise to the refluxing mixture until the color changed from red to green. The mixture was cooled to room temperature, and saturated KI solution was added until the product started to precipitate. The product was filtered off, washed with ether, and dried *in vacuo* affording quaternary ammonium salts **8–10** in good yield.

##### 4.6.1. 1-Ethyl-2-(2-dimethylaminovinyl)benz[*c,d*]indolium iodide (**8**)

Yield 76%, mp 242–244 °C; <sup>1</sup>H NMR (300 MHz, DMSO-*d*<sub>6</sub>) δ 1.56 (t, *J* = 7.0 Hz, 3H), 4.46 (s, 3H), 4.71 (q, *J* = 7.0 Hz, 2H), 8.00 (m, 1H), 8.19 (m, 1H), 8.45 (d, *J* = 8.0 Hz, 1H), 8.54 (d, *J* = 8.0 Hz, 1H), 8.69 (d, *J* = 8.0 Hz, 1H), 8.79 (d, *J* = 8.0 Hz, 1H).

##### 4.6.2. 1-Butyl-2-(2-dimethylaminovinyl)benz[*c,d*]indolium iodide, (**9**)

Yield 82%, <sup>1</sup>H NMR (400 MHz, DMSO-*d*<sub>6</sub>) δ 0.86 (t, *J* = 7.5 Hz, 3H), 1.27 (m, 2H), 1.75 (s, 6H), 1.82 (p, *J* = 6.6 Hz, 2H), 4.39 (t, *J* = 7.5 Hz,

2H), 7.79 (t,  $J = 8.1$  Hz, 1H), 7.94 (t,  $J = 7.5$  Hz, 1H), 8.02 (d,  $J = 7.2$  Hz, 1H), 8.07 (d,  $J = 8.4$  Hz, 1H), 8.45 (d,  $J = 8.1$  Hz, 1H), 8.91 (d,  $J = 7.2$  Hz, 1H).

#### 4.6.3. 1-Phenylpropyl-2-(2-dimethylaminovinyl)benz[c,d]indolium iodide (**10**)

Yield 86%, mp 75–76 °C;  $^1\text{H}$  NMR (400 MHz, DMSO- $d_6$ )  $\delta$  2.26 (m, 2H), 2.28 (t,  $J = 7.0$  Hz, 2H), 4.00 (s, 3H), 4.70 (t,  $J = 7.0$  Hz, 2H), 7.14 (m, 5H), 7.96 (t,  $J = 7.5$  Hz, 1H), 8.10 (t,  $J = 7.5$  Hz, 1H), 8.41 (m, 2H), 8.48 (d,  $J = 8.0$  Hz, 1H), 8.92 (d,  $J = 8.0$  Hz, 1H).

#### 4.7. General synthetic strategy for final dye compounds **11–13**

A mixture of the individual salts **8–10** (0.5 mmol), triethylformate (0.25 mmol), anhydrous sodium acetate (30 mg) and 4 mL of acetic anhydride was boiled for 1 h. The dye was suction filtered, washed with ethyl ether and dried.

##### 4.7.1. 1-Ethyl-2-[3-(1-ethylbenz[c,d]indol-2(1H)-ylidene)-1-propen-1-yl]-iodide (**11**)

Yield 75%;  $^1\text{H}$  NMR (400 MHz, DMSO- $d_6$ )  $\delta$  1.40 (t,  $J = 7.0$  Hz, 3H), 4.36 (d,  $J = 7.0$  Hz, 2H), 6.90 (d,  $J = 13.0$  Hz, 1H), 7.20 (m, 1H), 7.57 (d,  $J = 7.5$  Hz, 1H), 7.66 (t,  $J = 7.5$  Hz, 1H), 7.80 (d,  $J = 8.1$  Hz, 1H), 7.97 (t,  $J = 7.5$  Hz, 1H), 8.27 (d,  $J = 8.1$  Hz, 1H), 8.78 (t,  $J = 13.0$  Hz, 1H), 8.94 (d,  $J = 7.5$  Hz, 1H).  $^{13}\text{C}$  NMR (100 MHz, DMSO- $d_6$ )  $\delta$  14.56, 111.15, 111.50, 124.20, 124.81, 129.56, 129.94, 130.04, 130.08, 130.17, 130.92, 132.41, 140.64, 148.84, 155.18. TOF HRMS  $m/z$  ( $M^+$ ) calculated for  $\text{C}_{29}\text{H}_{25}\text{N}_2$  401.2018, found 401.2000.  $\lambda_{\text{max/em}}$  = 758/774 nm in methanol.

##### 4.7.2. 1-Butyl-2-[3-(1-butylbenz[c,d]indol-2(1H)-ylidene)-1-propen-1-yl]-iodide (**12**)

Yield 60%,  $^1\text{H}$  NMR (300 MHz, DMSO- $d_6$ )  $\delta$  0.96 (t,  $J = 7.2$  Hz, 6H), 1.43–1.50 (m, 4H), 1.85 (p,  $J = 6.9$  Hz, 4H), 4.40 (t,  $J = 6.6$  Hz, 4H), 7.23 (d,  $J = 13.2$  Hz, 4H), 7.72–7.77 (m, 4H), 7.86–7.90 (m, 4H), 8.06 (t,  $J = 7.5$  Hz, 2H), 8.36 (d,  $J = 8.1$  Hz, 1H), 8.66 (d,  $J = 7.2$  Hz, 2H), 9.20 (t,  $J = 13.2$  Hz, 1H).  $^{13}\text{C}$  NMR (100 MHz, DMSO- $d_6$ )  $\delta$  14.22, 20.14, 31.31, 44.30, 111.29, 111.74, 124.19, 124.69, 129.56, 129.92, 130.15, 130.27, 130.92, 132.41, 141.28, 148.96, 155.63. TOF HRMS  $m/z$  ( $M^+$ ) calculated for  $\text{C}_{33}\text{H}_{33}\text{N}_2$  457.2644, found 457.2624.  $\lambda_{\text{max/em}}$  = 758/774 nm in methanol.

##### 4.7.3. 1-Phenylpropyl-2-[3-(1-phenylpropylbenz[c,d]indol-2(1H)-ylidene)-1-propen-1-yl]iodide (**13**)

Yield 48%,  $^1\text{H}$  NMR (400 MHz, DMSO- $d_6$ )  $\delta$  2.06 (m, 2H), 2.75 (t,  $J = 7$  Hz, 2H), 4.27 (t,  $J = 7.0$  Hz, 2H), 6.75 (d,  $J = 13.6$  Hz, 1H), 6.97 (m, 1H), 7.24 (m, 5H), 7.46 (d,  $J = 7.5$  Hz, 1H), 7.63 (t,  $J = 8.0$  Hz, 1H), 7.76 (d,  $J = 8$  Hz, 1H), 7.94 (t,  $J = 7.5$  Hz, 1H), 8.25 (d,  $J = 8.0$  Hz, 1H), 8.73 (t,  $J = 13.0$  Hz, 1H), 8.87 (d,  $J = 8.0$  Hz, 1H).  $^{13}\text{C}$  NMR (100 MHz, DMSO- $d_6$ )  $\delta$  30.64, 32.69, 44.16, 111.21, 111.67, 124.22, 124.72, 126.49, 128.55, 128.68, 128.84, 129.52, 129.90, 130.12, 130.23, 130.93, 132.44, 141.19, 141.31, 148.85, 155.66. TOF HRMS  $m/z$  ( $M^+$ ) calculated for  $\text{C}_{43}\text{H}_{37}\text{N}_2$  581.2957, found 581.2934.  $\lambda_{\text{max/em}}$  = 758/774 nm in methanol.

#### 4.8. General synthesis of indolium and benz[e]indolium salts **16–21**

A mixture of indolenine **14** or **15** (31.4 mmol) and alkyl halide (94.2 mmol) were refluxed in acetonitrile (25 mL) for 24 h. The solvent was concentrated and removed *in vacuo* to afford an oil residue. The reaction mixture was cooled in an ice bath and solid was obtained upon addition of ether and acetone. The resulting crystals were filtered and dried to yield red to light pink solid which was used without further purification in subsequent reactions.

##### 4.8.1. 1-Ethyl-2,3,3-trimethyl-3H-indol-1-ium iodide (**16**)

This compound was obtained in 82% yield; mp 217–221 °C; (reported: mp 165–166 °C) [39].

##### 4.8.2. 1-Butyl-2,3,3-trimethyl-3H-indol-1-ium iodide (**17**)

This compound was obtained in 80% yield; mp 116–119 °C; (reported: yield 83%, mp 102 °C) [40].

##### 4.8.3. 2,3,3-Trimethyl-1-(3-phenylpropyl)-3H-indol-1-ium bromide (**18**)

81% yield; mp 169–171 °C;  $^1\text{H}$  NMR (400 MHz, MeOD- $d_4$ )  $\delta$  1.58 (s, 6H), 2.32 (p,  $J = 7.6$  Hz, 2H), 2.90 (t,  $J = 7.6$  Hz, 2H), 4.53 (t,  $J = 8.0$  Hz, 2H), 7.23–7.26 (m, 1H), 7.32–7.34 (m, 4H), 7.63–7.66 (m, 2H), 7.72–7.76 (m, 2H).

##### 4.8.4. 3-Ethyl-1,1,2-trimethyl-1H-benzo[e]indol-3-ium iodide (**19**)

This compound was obtained in 81% yield; mp 225–227 °C; (reported: yield 73%, mp 228 °C) [41].

##### 4.8.5. 3-Butyl-1,1,2-trimethyl-1H-benzo[e]indol-3-ium iodide (**20**)

This compound was obtained in 87% yield; mp 142–145 °C; (reported: yield 90%, mp 127–129) [42].

##### 4.8.6. 1,1,2-Trimethyl-3-(3-phenylpropyl)-1H-benzo[e]indol-3-ium iodide (**21**)

Yield 81%, mp 169–171 °C;  $^1\text{H}$  NMR (400 MHz, MeOD- $d_4$ )  $\delta$  1.58 (s, 6H), 2.32 (p,  $J = 7.6$  Hz, 2H), 2.90 (t,  $J = 7.6$  Hz, 2H), 4.53 (t,  $J = 8.0$  Hz, 2H), 7.23–7.26 (m, 1H), 7.32–7.34 (m, 4H), 7.63–7.66 (m, 2H), 7.72–7.76 (m, 2H).

#### 4.9. General synthesis of **22–27**

Quaternized ammonium salts **16–21** were heated to 80 °C in acetic anhydride. Triethyl orthoformate was added to the reaction mixture causing an instant color change to deep purple. The reaction mixture was monitored by UV/Vis spectroscopy in methanol and TLC analysis using DCM as the mobile phase. After 2 h the reaction was stopped and the flask was cooled in a freezer. After 5–10 h, the product precipitated was filtered and dried. Initial product purification was performed by recrystallization using minimum amounts of methanol, reduced temperature, and titration with ether. Compounds **24**, **26** and **27** were additionally purified using silica gel and 2% MeOH in dichloromethane as eluting solvent.

##### 4.9.1. 1-Ethyl-2-((1E,3E)-3-(1-ethyl-3,3-dimethylindolin-2-ylidene)prop-1-en-1-yl)-3,3-dimethyl-3H-indolium iodide (**22**)

Yield 77%,  $^1\text{H}$  NMR (400 MHz, MeOD- $d_4$ )  $\delta$  1.43 (t,  $J = 8.0$  Hz, 6H), 1.77 (s, 12H), 4.22 (q,  $J = 8.0$  Hz, 4H), 6.53 (d,  $J = 12.0$  Hz, 2H), 7.31 (t,  $J = 8.0$  Hz, 2H), 7.36 (d,  $J = 8.0$  Hz, 2H), 7.45 (t,  $J = 8.0$  Hz, 2H), 7.55 (d,  $J = 8.0$  Hz, 2H), 8.56 (t,  $J = 12.0$  Hz, 1H);  $^{13}\text{C}$  NMR (100 MHz, MeOD- $d_4$ )  $\delta$  12.69, 28.25, 40.35, 103.44, 112.23, 123.60, 126.77, 130.04, 142.34, 142.95, 152.32, 175.63; TOF HRMS  $m/z$  ( $M^+$ ) calculated for  $\text{C}_{27}\text{H}_{33}\text{N}_2$  385.2644, found 385.2647.  $\lambda_{\text{max/em}}$  = 546/561 nm in methanol.

##### 4.9.2. 1-Butyl-2-((1E,3E)-3-(1-butyl-3,3-dimethylindolin-2-ylidene)prop-1-en-1-yl)-3,3-dimethyl-3H-indol-1-ium (**23**)

Yield 74%, mp 172–175 °C;  $^1\text{H}$  NMR (400 MHz, DMSO)  $\delta$  0.95 (t,  $J = 8.0$  Hz, 6H), 1.41–1.54 (m, 4H), 1.71 (s, 12H), 1.68–1.80 (m, 4H), 4.14 (t,  $J = 8.0$  Hz, 4H), 6.52 (d,  $J = 16.0$  Hz, 2H), 7.31 (t,  $J = 8.0$  Hz, 2H), 7.46 (q,  $J = 8.0$  Hz, 4H), 7.65 (d,  $J = 16.0$  Hz, 2H), 8.37 (t,  $J = 12.0$  Hz, 1H);  $^{13}\text{C}$  NMR (MeOD- $d_4$ )  $\delta$  13.81, 19.57, 27.46, 29.21, 43.70, 48.90, 102.50, 111.56, 122.50, 125.20, 128.64, 140.61, 141.87, 173.84; TOF HRMS  $m/z$  ( $M^+$ ) calculated for  $\text{C}_{31}\text{H}_{41}\text{N}_2$  441.3270, found 441.3279.  $\lambda_{\text{max/em}}$  = 546/561 nm in methanol.

#### 4.9.3. 1-Phenylpropyl-2-((1E,3E)-3-(1-butyl-3,3-dimethylindolin-2-ylidene)prop-1-en-1-yl)-3,3-dimethyl-3H-indol-1-ium (**24**)

Yield 67%, mp 255–258 °C; <sup>1</sup>H NMR (400 MHz, MeOD-*d*<sub>4</sub>) δ 1.74 (s, 12H), 2.18 (p, *J* = 7.2 Hz, 4H), 2.85 (t, *J* = 7.5 Hz, 4H), 4.18 (t, *J* = 7.8 Hz, 4H), 6.21 (d, *J* = 13.3 Hz, 2H), 7.45 (t, *J* = 8.0 Hz, 2H), 7.55 (d, *J* = 8.0 Hz, 2H), 8.56 (t, *J* = 12.0 Hz, 1H); <sup>13</sup>C NMR (100 MHz, MeOD-*d*<sub>4</sub>) δ 24.64, 28.30, 29.97, 33.74, 44.65, 103.69, 112.37, 123.56, 126.82, 127.45, 129.61, 129.71, 129.98, 142.08, 142.21, 143.27, 175.96; TOF HRMS *m/z* (*M*<sup>+</sup>) calculated for C<sub>27</sub>H<sub>33</sub>N<sub>2</sub> 385.2644, found 385.2647. λ<sub>max/em</sub> = 546/561 nm in methanol.

#### 4.9.4. 3-Ethyl-2-((1E,3E)-3-(3-ethyl-1,1-dimethyl-1H-benzo[e]indol-2(3H)-ylidene)prop-1-en-1-yl)-1,1-dimethyl-1H-benzo[e]indol-3-ium iodide (**25**)

Yield 66%, mp >260 °C; <sup>1</sup>H NMR (400 MHz, MeOD-*d*<sub>4</sub>) δ 1.50 (t, *J* = 8.0 Hz, 6H), 2.10 (s, 12H), 4.34 (q, *J* = 8.0 Hz, 4H), 6.53 (d, *J* = 16.0 Hz, 2H), 7.53 (t, *J* = 8.0 Hz, 2H), 7.65 (d, *J* = 8.0 Hz, 2H), 7.67 (d, *J* = 8.0 Hz, 2H), 8.03 (d, *J* = 8.0 Hz, 2H), 8.065 (d, *J* = 12.0 Hz, 2H), 8.295 (d, *J* = 8.0 Hz, 2H), 8.79 (t, *J* = 8.0 Hz, 1H); <sup>13</sup>C NMR (100 MHz, MeOD-*d*<sub>4</sub>) δ 13.13, 28.07, 40.68, 52.59, 102.96, 112.14, 123.49, 126.49, 129.07, 129.55, 131.34, 132.16, 133.82, 140.59; TOF HRMS *m/z* (*M*<sup>+</sup>) calculated for C<sub>35</sub>H<sub>37</sub>N<sub>2</sub> 485.2957, found 485.2960. λ<sub>max/em</sub> = 586/605 nm in methanol.

#### 4.9.5. 3-Butyl-2-((1E,3E)-3-(3-butyl-1,1-dimethyl-1H-benzo[e]indol-2(3H)-ylidene)prop-1-en-1-yl)-1,1-dimethyl-1H-benzo[e]indol-3-ium iodide (**26**)

Yield 63%, <sup>1</sup>H NMR (400 MHz, MeOD-*d*<sub>4</sub>) δ 1.06 (t, *J* = 8.0 Hz, 6H), 1.55–1.61 (m, 4H), 1.88–1.94 (m, 4H), 2.11 (s, 12H), 4.20 (t, *J* = 8.0 Hz, 4H), 6.565 (d, *J* = 12.0 Hz, 2H), 7.53 (t, *J* = 8.0 Hz, 2H), 7.64 (d, *J* = 8.0 Hz, 2H), 7.69 (t, *J* = 12.0 Hz, 2H), 8.03 (d, *J* = 8.0 Hz, 2H), 8.06 (d, *J* = 8.0 Hz, 2H), 8.30 (d, *J* = 8.0 Hz, 2H), 8.79 (t, *J* = 12.0 Hz, 1H); <sup>13</sup>C NMR (100 MHz, MeOD-*d*<sub>4</sub>) δ 14.41, 21.11, 21.36, 28.18, 31.13, 52.56, 103.27, 112.37, 123.50, 126.52, 129.09, 129.48, 131.34, 132.10, 133.80, 135.10, 141.02; TOF HRMS *m/z* (*M*<sup>+</sup>) calculated for C<sub>39</sub>H<sub>45</sub>N<sub>2</sub> 541.3583, found 541.3582. λ<sub>max/em</sub> = 586/605 nm in methanol.

#### 4.9.6. 2-((1E,3E)-3-(1,1-Dimethyl-3-(3-phenylpropyl)-1H-benzo[e]indol-2(3H)-ylidene)prop-1-en-1-yl)-1,1-dimethyl-3-(3-phenylpropyl)-1H-benzo[e]indol-3-ium iodide (**27**)

Yield 55%, <sup>1</sup>H NMR (400 MHz, MeOD-*d*<sub>4</sub>) δ 2.01 (s, 12H), 2.12 (p, *J* = 8.0 Hz, 4H), 2.82 (t, *J* = 8.0 Hz, 4H), 4.31 (t, *J* = 8.0 Hz, 4H), 6.395 (d, *J* = 12.0 Hz, 2H), 7.21–7.33 (m, 12H), 7.55 (t, *J* = 8.0 Hz, 2H), 7.740 (t, *J* = 8.0 Hz, 2H), 7.75 (d, *J* = 8.0 Hz, 2H), 8.11 (t, *J* = 8.0 Hz, 4H), 8.30 (d, *J* = 8.0 Hz, 2H), 8.58 (t, *J* = 12.0 Hz, 1H); <sup>13</sup>C NMR (100 MHz, MeOD-*d*<sub>4</sub>) δ 26.60, 28.76, 32.32, 101.59, 110.65, 121.92, 125.01, 126.08, 127.55, 127.90, 127.99, 128.07, 128.21, 128.34, 129.78, 130.55, 132.27, 139.29, 140.62. TOF HRMS *m/z* (*M*<sup>+</sup>) calculated for C<sub>49</sub>H<sub>49</sub>N<sub>2</sub> 665.3896, found 665.3893. λ<sub>max/em</sub> = 586/605 nm in methanol.

#### 4.10. Protein expression and purification

PRMT1-pET28b plasmid was transformed into *E. coli* BL21 (DE3) using heat shock method. Protein expression was induced with 0.3-mM IPTG at 16 °C for 20 h. After protein expression, cells were pelleted by centrifuge followed by suspension in the lysis buffer (25 mM HEPES pH 8.0, 150 mM NaCl, 1 mM PMSF, 1 mM MgSO<sub>4</sub>, 5% glycerol, 5% ethylene glycol) and lysed by French Press. The protein supernatant was purified on the Ni-charged His-tag binding resin (Novagen). The beads were equilibrated with column buffer (25 mM Na-HEPES pH 8.0, 500 mM NaCl, 1 mM PMSF, and 30 mM imidazole, 10% glycerol, 1 mM PMSF) followed by protein loading. After that the beads were washed thoroughly with the column buffer, and then the protein was eluted with the elution buffer

(25 mM Na-HEPES, pH 7.0, 300 mM NaCl, 1 mM PMSF, 100 mM EDTA and 200 mM imidazole, 5% glycerol). Different elution fractions were checked on SDS–PAGE. Then, protein fractions were combined and dialyzed against the storage buffer (25 mM Na-HEPES, pH 7.0, 500 mM NaCl, 1 mM EDTA, 10 mM DTT and 10% glycerol) at 4 °C. After dialysis, the protein solution was concentrated using Millipore centrifugal filters. His6x-tagged PRMT3 was expressed from the pReceiver vector. GST-mCARM1 was expressed from the pGEX-4T1 vector. His6x-tagged PRMT5 and PRMT6 were expressed from the pET28a vector. All of the proteins were expressed in *E. coli* BL21(DE3). All of the His6x-tagged proteins were purified on Ni-NTA beads. Protein concentrations were determined using Bradford assay.

#### 4.11. Radioactive methyltransferase assay

The inhibitory activities of small molecule compounds were examined by using <sup>14</sup>C-labeled radioactive methylation assays. The assays were carried out in 0.6 mL plastic tubes at 30 °C in a reaction volume of 30 μL. The reaction buffer contained 50 mM HEPES (pH 8.0), 0.5 mM dithiothreitol (DTT), 1 mM EDTA, and 50 mM NaCl. In a typical procedure, peptide substrate, [<sup>14</sup>C]-S-Adenosyl-L-methionine and inhibitor were preincubated in the reaction buffer for 5 min prior to the initiation by the addition of PRMT1 (0.05 μM final). After it was incubated for 8 min, the reaction was quenched by spreading the reaction mixture onto P81 filter paper discs (Whatman). The paper disk was washed with 50 mM NaHCO<sub>3</sub>, and dried in air for 2 h. The amount of methylated products was quantified by liquid scintillation. To determine the IC<sub>50</sub> value of those inhibitors similar experiment was performed with H4-(1–20) (2 μM), [<sup>14</sup>C]-S-Adenosyl-L-methionine (5 μM) and DMSO (2%) and varied concentration of inhibitors. The IC<sub>50</sub> value is the concentration of inhibitor at which half of the maximal activity is reached. The inhibition patterns of **11** were determined by measuring initial velocities of PRMT1 at a range of varied concentrations of one substrate, a fixed concentration of the other substrate, and selected concentrations of the inhibitors. The data were displayed in double reciprocal formats and fitted to competitive or noncompetitive kinetic equations.

#### 4.12. Time-dependent inhibition assay

Depending upon the IC<sub>50</sub> value of the compound, different concentrations of the compound were incubated with 0.05 μM enzyme so that in the final reaction mixture **11** was present at 0, 1.5, 2.5, 4.0 μM. Incubations were conducted for 0, 2, 4, 6, 8, 10, 15, 20, 25, 30 min at 30 °C. After each incubation, the reaction was quenched by spreading 20 μL reaction mixture onto P81 filter paper discs (Whatman).

#### 4.13. Dialysis experiment

For the dialysis assay, 1 μM PRMT1 was incubated with 20 μM **11** in a total reaction volume of 520 μL for 1 h at 30 °C to achieve complete inactivation. Enzyme without any inhibitor was used in experimental controls. The reaction mixtures were then transferred to dialysis cassettes (molecular weight cut off of 10 000Da) and dialyzed for 3 days at 4 °C in the 300 mL reaction buffer contained 50 mM HEPES (pH 8.0), 0.5 mM dithiothreitol (DTT), 1 mM EDTA, 50 mM NaCl and 10% DMSO. The buffer was changed six times during this period. After finishing dialysis, residual activity assays were performed on pre- and post-dialysis samples. The activity was measured in the presence of 2 μM peptide substrate, 5 μM [<sup>14</sup>C]-S-Adenosyl-L-methionine and dialyzed samples were preincubated in the reaction buffer for 5 min prior to the initiation by the addition

of PRMT1 (0.05  $\mu$ M final). After it was incubated for 8 min, the reaction was quenched by spreading the reaction mixture onto P81 filter paper discs (Whatman). The paper discs were washed with 50 mM NaHCO<sub>3</sub> and dried in air for 2 h. The amount of methylated products was quantified by liquid scintillation. The amount of product formed in the control reaction was set as 100% and used to determine the percent activity remaining in the inhibited reactions.

#### 4.14. Bright field and fluorescent microscopic imaging

HeLa cells were seeded on coverglass overnight and treated without or with different concentrations of **11** for 6 h. Cells were then fixed by 4% paraformaldehyde for 10 min at room temperature. Then the optical images were taken under visible light by CoolSNAP CF camera attached to a Nikon Ti-80 microscope. The NIR fluorescent images were taken by an LSM META NLO confocal microscope (Creighton university Integrated biomedical imaging Facility) using a 633-nm laser and a 715–785-nm Long Pass filter.

#### 4.15. Antiproliferative assay of HeLa cells

HeLa cells were maintained in Dulbecco's modified Eagle's medium (DMEM) (Cellgro) supplemented with 10% fetal bovine serum (Cellgro) and 1% penicillin–streptomycin in 5% CO<sub>2</sub> at 37 °C. Cells were washed with PBS and harvested using trypsin. Individual wells of a 96-well tissue culture plate were inoculated with 100  $\mu$ L of complete medium containing 9000 cells and incubated overnight for attachment at 37 °C in a 5% CO<sub>2</sub> incubator. The following day, the media were removed and the cells were treated with different concentrations of **11**. The final concentration of DMSO in the culture medium was maintained at 0.2%. Control cells (without any compound) were treated under the same conditions. After 48 h of incubation period, cell survival was evaluated using an MTT assay: 10  $\mu$ L of a freshly prepared solution of MTT (5 mg/mL in PBS) was added to each well, and after 4 h of incubation, the medium was removed; after addition of 100  $\mu$ L of DMSO to each well, the optical density values were detected at 530 nm. Cytotoxicity data were expressed as IC<sub>50</sub> values. Data were expressed as mean values of three individual experiments conducted in triplicate.

#### 4.16. Cell cycle assay

For flow cytometric analysis of DNA content,  $1 \times 10^6$  cells in exponential growth were treated with different concentrations of **11** at different concentrations for 24 and 48 h. After the incubation, the cells were collected, centrifuged and fixed with ice-cold ethanol (70%) and stored at 4 °C until use. Subsequently, cells were rinsed with PBS and stained with PBS containing 40  $\mu$ g/mL propidium iodide and followed by the addition of RNase A. Samples were analyzed on a BD-LRFortessa flow cytometer (BD Biosciences). For cell cycle analysis, DNA histograms were analyzed using Flow Jo software.

#### Acknowledgments

This work is supported by Georgia Cancer Coalition Distinguished Cancer Scholar Award and NIH Grant GM086717 to YGZ. YF is supported by an American Heart Association Pre-doctoral Fellowship and a University Doctoral Fellowship at GSU under the instruction of YGZ. The synthesis of inhibitors was supported by the GSU Research Initiation Grant and Georgia Cancer Coalition Grant to MH. Additionally, MH would like to acknowledge the Center for Diagnostics and Therapeutics at Georgia State University for the support.

#### Appendix A. Supplementary information

Supplementary data associated with this article can be found, in the online version, at <http://dx.doi.org/10.1016/j.ejmech.2012.06.017>.

#### References

- [1] A. Di Lorenzo, M.T. Bedford, Histone arginine methylation, *FEBS Lett.* 585 (2011) 2024–2031.
- [2] S.S. Wolf, The protein arginine methyltransferase family: an update about function, new perspectives and the physiological role in humans, *Cell. Mol. Life Sci.* 66 (2009) 2109–2121.
- [3] C.D. Krause, Z.H. Yang, Y.S. Kim, J.H. Lee, J.R. Cook, S. Pestka, Protein arginine methyltransferases: evolution and assessment of their pharmacological and therapeutic potential, *Pharmacol. Ther.* 113 (2007) 50–87.
- [4] S. Pal, S. Sif, Interplay between chromatin remodelers and protein arginine methyltransferases, *J. Cell. Physiol.* 213 (2007) 306–315.
- [5] N. Cheung, L.C. Chan, A. Thompson, M.L. Cleary, C.W. So, Protein arginine-methyltransferase-dependent oncogenesis, *Nat. Cell. Biol.* 9 (2007) 1208–1215.
- [6] D. Zakrzewicz, O. Eickelberg, From arginine methylation to ADMA: a novel mechanism with therapeutic potential in chronic lung diseases, *BMC Pulm. Med.* 9 (2009) 5.
- [7] J. Beltowski, A. Kedra, Asymmetric dimethylarginine (ADMA) as a target for pharmacotherapy, *Pharmacol. Rep.* 58 (2006) 159–178.
- [8] R. Maas, Pharmacotherapies and their influence on asymmetric dimethylarginine (ADMA), *Vasc. Med.* 10 (Suppl. 1) (2005) S49–S57.
- [9] S.S. Koh, D. Chen, Y.H. Lee, M.R. Stallcup, Synergistic enhancement of nuclear receptor function by p160 coactivators and two coactivators with protein methyltransferase activities, *J. Biol. Chem.* 276 (2001) 1089–1098.
- [10] S. Wagner, S. Weber, M.A. Kleinschmidt, K. Nagata, U.M. Bauer, SET-mediated promoter hypoacetylation is a prerequisite for coactivation of the estrogen-responsive pS2 gene by PRMT1, *J. Biol. Chem.* 281 (2006) 27242–27250.
- [11] I. Goulet, G. Gauvin, S. Boisvenue, J. Cote, Alternative splicing yields protein arginine methyltransferase 1 isoforms with distinct activity, substrate specificity, and subcellular localization, *J. Biol. Chem.* 282 (2007) 33009–33021.
- [12] K. Mathioudaki, A. Scorilas, A. Ardavanis, P. Lymberi, E. Tsiambas, M. Devetzi, A. Apostolaki, M. Talieri, Clinical evaluation of PRMT1 gene expression in breast cancer, *Tumour Biol.* 32 (2011) 575–582.
- [13] A. Papadokostopoulou, K. Mathioudaki, A. Scorilas, D. Xynopoulos, A. Ardavanis, E. Kouroumalis, M. Talieri, Colon cancer and protein arginine methyltransferase 1 gene expression, *Anticancer Res.* 29 (2009) 1361–1366.
- [14] Y.G. Zheng, J. Wu, Z. Chen, M. Goodman, Chemical regulation of epigenetic modifications: opportunities for new cancer therapy, *Med. Res. Rev.* 28 (2008) 645–687.
- [15] A. Spannhoff, A.T. Hauser, R. Heinke, W. Sippl, M. Jung, The emerging therapeutic potential of histone methyltransferase and demethylase inhibitors, *ChemMedChem* 4 (2009) 1568–1582.
- [16] A. Spannhoff, R. Heinke, I. Bauer, P. Trojer, E. Metzger, R. Gust, R. Schüle, G. Brosch, W. Sippl, M. Jung, Target-based approach to inhibitors of histone arginine methyltransferases, *J. Med. Chem.* 50 (2007) 2319–2325.
- [17] A. Spannhoff, R. Machmur, R. Heinke, P. Trojer, I. Bauer, G. Brosch, R. Schüle, W. Hanefeld, W. Sippl, M.A. Jung, A novel arginine methyltransferase inhibitor with cellular activity, *Bioorg. Med. Chem. Lett.* 17 (2007) 4150–4153.
- [18] R. Ragno, S. Simeoni, S. Castellano, C. Vicidomini, A. Mai, A. Caroli, A. Tramontano, C. Bonaccini, P. Trojer, I. Bauer, G. Brosch, G. Sbardella, Small molecule inhibitors of histone arginine methyltransferases: homology modeling, molecular docking, binding mode analysis, and biological evaluations, *J. Med. Chem.* 50 (2007) 1241–1253.
- [19] A. Mai, D. Cheng, M.T. Bedford, M.S. Valente, A. Nebbioso, A. Perrone, G. Brosch, G. Sbardella, F. De Bellis, M. Miceli, L. Altucci, Epigenetic multiple ligands: mixed histone/protein methyltransferase, acetyltransferase, and class III deacetylase (Sirtuin) inhibitors, *J. Med. Chem.* 51 (2008) 2279–2290.
- [20] D. Cheng, N. Yadav, R.W. King, M.S. Swanson, E.J. Weinstein, M.T. Bedford, Small molecule regulators of protein arginine methyltransferases, *J. Biol. Chem.* 279 (2004) 23892–23899.
- [21] M.T. Bedford, S. Richard, Arginine methylation: an emerging regulator of protein function, *Mol. Cell* 18 (2005) 263–272.
- [22] K.K. Li, C. Luo, D. Wang, H. Jiang, Y.G. Zheng, Chemical and biochemical approaches in the study of histone methylation and demethylation, *Med. Res. Rev.* (2010).
- [23] E.-M. Bissinger, R. Heinke, A. Spannhoff, A. Eberlin, E. Metzger, V. Cura, P. Hassenboehler, J. Cavarelli, R. Schüle, M.T. Bedford, W. Sippl, M. Jung, Acyl derivatives of p-aminosulfonamides and dapsons as new inhibitors of the arginine methyltransferase hPRMT1, *Bioorg. Med. Chem.* 19 (2011) 3717–3731.
- [24] Y. Feng, M. Li, B. Wang, Y.G. Zheng, Discovery and mechanistic study of a class of protein arginine methylation inhibitors, *J. Med. Chem.* 53 (2010) 6028–6039.

- [25] D. Cheng, S. Valente, S. Castellano, G. Sbardella, R. Di Santo, R. Costi, M.T. Bedford, A. Mai, Novel 3,5-bis(bromohydroxybenzylidene)piperidin-4-ones as coactivator-associated arginine methyltransferase 1 inhibitors: enzyme selectivity and cellular activity, *J. Med. Chem.* 54 (2011) 4928–4932.
- [26] D. Cheng, M.T. Bedford, Xenoestrogens regulate the activity of arginine methyltransferases, *ChemBioChem* 12 (2011) 323–329.
- [27] R. Heinke, A. Spannhoff, R. Meier, P. Trojer, I. Bauer, M. Jung, W. Sippl, Virtual screening and biological characterization of novel histone arginine methyltransferase PRMT1 inhibitors, *ChemMedChem* 4 (2009) 69–77.
- [28] J. Dowden, R.A. Pike, R.V. Parry, W. Hong, U.A. Muhsen, S.G. Ward, Small molecule inhibitors that discriminate between protein arginine *N*-methyltransferases PRMT1 and CARM1, *Org. Biomol. Chem.* 9 (2011) 7814–7821.
- [29] L. Strekowski, C.J. Mason, H. Lee, R. Gupta, J. Sowell, G. Patonay, Synthesis of water-soluble near-infrared cyanine dyes functionalized with [(succinimido)oxy]carbonyl group, *J. Heterocycl. Chem.* 40 (2003) 913–916.
- [30] A. Mishra, R.K. Behera, P.K. Behera, B.K. Mishra, G.B. Behera, Cyanines during the 1990s: a review, *Chem. Rev.* 100 (2000) 1973–2012.
- [31] N. Narayanan, G. Patonay, A new method for the synthesis of heptamethine cyanine dyes: synthesis of new near-infrared fluorescent labels, *J. Org. Chem.* 60 (1995) 2391–2395.
- [32] M. Mojzych, M. Henary, Synthesis of cyanine dyes, in: L. Strekowski (Ed.), *Heterocyclic Polymethine Dyes* (2008), pp. 1–9.
- [33] M.Y. Losytskyy, K.D. Volkova, V.B. Kovalska, I.E. Makovenko, Y.L. Slominskii, O.I. Tolmachev, S.M. Yarmoluk, Fluorescent properties of pentamethine cyanine dyes with cyclopentene and cyclohexene group in presence of biological markers, *J. Fluoresc.* 15 (2005) 849–857.
- [34] J.H. Flanagan, S. Khan, S. Menchen, S.A. Soper, R.P. Hammer, Functionalized tricarbo-cyanine dyes as near-infrared fluorescent probes for biomolecules, *Bioconjugate Chem.* 8 (1997) 751–756.
- [35] N.P. Vasilenko, F.A. Mikhailenko, Y.I. Rozhinskii, 2-Methylbenz[c,d]indole and its derivatives, *Dyes Pigm.* 2 (1981) 231–237.
- [36] G.E. Ficken, J.D. Kendall, The reactivity of the alkylthio group in nitrogen ring compounds. III. 2-Methylthiobenz[c,d]indole and its methiodide, *J. Chem. Soc.* (1960) 1537–1541.
- [37] M.V. Lakshmikantham, W. Chen, M.P. Cava, Thioanhydrides. 3. Synthesis, properties, and Diels-Alder reactions of sulfur analogues of 1,8-naphthalic anhydride, *J. Org. Chem.* 54 (1989) 4746–4750.
- [38] T.G. Deligeorgiev, N.I. Gadjev, Styryl dyes containing the benz[c,d]indolium heterocycle, *Dyes Pigm.* 15 (1991) 215–223.
- [39] R.L. Simmons, R.T. Yu, A.G. Myers, Storable arylpalladium(II) reagents for alkene labeling in aqueous media, *J. Am. Chem. Soc.* 40 (2011) 15870–15873.
- [40] C.C. Lee, A.T. Hu, Synthesis and optical recording properties of some novel styryl dyes for DVD-R, *Dyes Pigm.* 59 (2003) 63–69.
- [41] S. Kuster, F. Sauvage, M.K. Nazeeruddin, M. Grätzel, F.A. Nüesch, T. Geiger, Unsymmetrical squaraine dimer with an extended  $\pi$ -electron framework: an approach in harvesting near infra-red photons for energy conversion, *Dyes Pigm.* 87 (2010) 30–38.
- [42] M.V. Kvach, A.V. Ustinov, I.A. Stepanova, A.D. Malakhov, M.V. Skorobogatyi, V.V. Shmanai, V.A. Korshun, A convenient synthesis of cyanine dyes: reagents for the labeling of biomolecules, *Eur. J. Org. Chem.* 12 (2008) 2107–2117.